S1 Summary statistics for RADM2 simulation against meteorological observations

Table S1: Domain-wide statistical performance of WRF-Chem RADM2 simulation against 3-hourly meteorological observations from BADC.

	Winter (DJF)							Spring (MAM)						
	Mean-Obs	Mean-Mod	MB	NMB	MFB	r	no. stations	Mean-Obs	Mean-Mod	MB	NMB	MFB	r	no. stations
MSLP (hPa)	1015.41	1014.79	-0.96	-0.00	-0.00	0.99	1297	1014.67	1014.46	-0.35	-0.00	-0.00	0.99	1295
T2 (° C)	2.51	2.99	0.29	0.11	0.26	0.89	1581	9.73	9.91	-0.11	-0.01	0.07	0.94	1581
WS10 (m/s)	4.31	5.60	1.34	0.31	0.42	0.71	1577	3.86	4.46	0.65	0.17	0.29	0.68	1589
WD10 (deg)	175.53	203.74	27.94	0.16	0.27	0.50	1568	167.88	188.67	21.16	0.13	0.25	0.48	1580
	Summer (JJA)							Fall (SON)						
	Mean-Obs	Mean-Mod	MB	NMB	MFB	r	no. stations	Mean-Obs	Mean-Mod	MB	NMB	MFB	r	no. stations
MSLP (hPa)	1012.12	1012.11	0.03	0.00	0.00	0.98	1288	1017.61	1017.42	-0.49	-0.00	-0.00	0.99	1297
T2 (° C)	17.82	17.80	-0.27	-0.02	-0.01	0.88	1573	9.20	9.66	0.25	0.03	0.47	0.95	1583
WS10 (m/s)	3.45	3.92	0.50	0.14	0.27	0.63	1574	3.64	4.61	1.04	0.28	0.40	0.68	1585
WD10 (deg)	173.88	197.03	23.38	0.13	0.25	0.45	1561	172.30	196.54	24.07	0.14	0.27	0.48	1574

S2 Differences in implementation of dry deposition and photolysis

The MOZART mechanism in WRF uses a version of the standard WRF-Chem implementation of the Wesley dry deposition scheme (based on Wesely, 1989; Erisman et al., 1994) that has been modified to include a more complex seasonal variation in the dry deposition rates than is used in the standard implementation. Specifically, in the MOZART implementation of dry deposition, five different seasons are used to describe the variation in plant functional type, whereas in the standard implementation used by RADM2, only two seasons (summer and winter) are used. Furthermore, within the dry deposition routine, MOZART uses slightly different values for effective Henry's Law coefficients and diffusion coefficients.

As indicated in Table 2 in the main text, the scheme used to calculate photolysis rates (J values) based on radiation differs in the MOZART and RADM2 simulations. RADM2 was run with the Madronich TUV scheme, whereas MOZART chemistry in WRF is designed to run with the Madronich FTUV scheme. The FTUV model has the same physical processes as the TUV model, except that the number of wavelength bins between 121 and 750 nm are 140 for TUV vs. 17 for FTUV, which speeds up computations and leads to differences in photolysis rates of less than 5% in the troposphere, as calculated by Tie et al. (2003). An additional difference is that when MOZART is run in WRF-Chem, the standard WRF-Chem FTUV scheme is further modified to read in climatological O_3 and O_2 overhead columns rather than using a fixed value.

S3 Differences in inorganic rate coefficients

Table S2: Inorganic rate coefficients used in RADM2 that, for a July sensitivity study, were changed to match those used for the equivalent reactions in MOZART. Chemical equations and rate coefficient expressions are shown in the syntax of the Kinetic Pre Processor used to generate model code.

Reaction	Rate coefficient in base simulation	Rate coefficient as changed to match MOZART
O3P+NO2=NO+O2	ARR2(6.5D-12, -120.0_dp, TEMP)	ARR2(5.6e-12_dp, -180.0_dp, TEMP)
O1D+M=O3P	.78084* ARR2(1.8D-11, -110.0_dp, TEMP) + .20946e0* ARR2(3.2D-11, -70.0_dp, TEMP)	.79_dp*ARR2(2.1e-11_dp, -115.0_dp, TEMP) + .21_dp*ARR2(3.2e-11_dp, -70.0_dp, TEMP)
O3+NO=NO2+O2	ARR2(2.0D-12, 1400.0_dp, TEMP)	ARR2(3.0e-12_dp, 1500.0_dp, TEMP)
O3+OH=HO2+O2	ARR2(1.6D-12, 940.0_dp, TEMP)	ARR2(1.7e-12_dp, 940.0_dp, TEMP)
O3+HO2=OH+2.00 O2	ARR2(1.1D-14, 500.0_dp, TEMP)	ARR2(1.0e-14_dp, 490.0_dp, TEMP)
HO2+NO=NO2+OH	ARR2(3.7D-12, -240.0_dp, TEMP)	ARR2(3.5e-12_dp, -250.0_dp, TEMP)
H2O2+OH=HO2+H2O	ARR2(3.3D-12, 200.0_dp, TEMP)	ARR2(2.9e-12_dp, 160.0_dp, TEMP)
O3+NO2=NO3	ARR2(1.4D-13, 2500.0_dp, TEMP)	ARR2(1.2e-13_dp, 2450.0_dp, TEMP)
NO3+NO=NO2+NO2	ARR2(1.7D-11, -150.0_dp, TEMP)	ARR2(1.5e-11_dp, -170._dp, TEMP)
NO3+NO2=N2O5	TROE(2.20D-30 , 4.3_dp , 1.50D-12 , 0.5_dp , TEMP, C_M)	TROE(2.e-30_dp , 4.4_dp , 1.4e-12_dp , .7_dp , TEMP, C_M)
OH+NO2=HNO3	TROE(2.60D-30 , 3.2_dp , 2.40D-11 , 1.3_dp , TEMP, C_M)	TROE(2.e-30_dp , 3._dp , 2.5e-11_dp , 0._dp , TEMP, C_M)
OH+HNO3=NO3+H2O	k46(TEMP,C_M)	usr5(TEMP, C_M)
OH+HO2=H2O+O2	ARR2(4.6D-11, -230.0_dp, TEMP)	ARR2(4.8e-11_dp, -250.0_dp, TEMP)
OH+SO2=SULF+HO2	TROE(3.00D-31 , 3.3_dp , 1.50D-12 , 0.0_dp , TEMP, C_M)	usr23(TEMP, C_M)
CO+OH=HO2+CO2	(1.5D-13 * (1._dp + 2.439D-20*C_M))	usr8(temp, C_M)

Definition of rate expressions in Table S2.

```
REAL(kind=dp) FUNCTION ARR2( A0,B0, TEMP )
REAL(kind=dp) :: TEMP
REAL(kind=dp) A0,B0
ARR2 = A0 * EXP( -B0 /TEMP )
END FUNCTION ARR2

REAL(KIND=dp) FUNCTION usr5( temp, C_M )
REAL(KIND=dp), INTENT(IN) :: temp
REAL(KIND=dp), INTENT(IN) :: C_M
REAL(KIND=dp) :: k0, k2
k0 = C_M * 6.5e-34_dp * exp( 1335._dp/temp )
k2 = exp( 2199._dp/temp )
k0 = k0 /(1.0_dp + k0/(2.7e-11_dp*k2))
k2 = exp( 460._dp/temp )
usr5 = k0 + 2.4e-14_dp * k2
END FUNCTION usr5

REAL(KIND=dp) FUNCTION usr23( temp, C_M )
REAL(KIND=dp), INTENT(IN) :: temp
REAL(KIND=dp), INTENT(IN) :: C_M
REAL(KIND=dp) :: fc, k0
REAL(KIND=dp) :: wrk
fc = 3.e-11_dp * (300._dp/temp) ** 3.3_dp
wrk = fc * C_M
k0 = wrk / (1._dp + wrk/1.5e-12_dp)
usr23 = k0 * .6_dp ** (1._dp/(1._dp + (log10( wrk/1.5e-12_dp ))**2._dp))
END FUNCTION usr23

REAL(KIND=dp) FUNCTION usr8( temp, C_M )
REAL(KIND=dp), INTENT(IN) :: temp
REAL(KIND=dp), INTENT(IN) :: C_M
```

```
54 REAL(KIND=dp), parameter :: boltz = 1.38044e-16_dp
55 usr8 = 1.5e-13_dp * (1._dp + 6.e-7_dp*boltz*C_M*temp)
56 END FUNCTION usr8
57
58 REAL(KIND=dp) FUNCTION k46( TEMP, C_M
59 REAL(KIND=dp), INTENT(IN) :: temp, C_M
60 REAL(KIND=dp) :: k0, k2, k3
61 k0=7.2E-15_dp * EXP(785._dp/TEMP)
62 k2=4.1E-16_dp * EXP(1440._dp/TEMP)
63 k3=1.9E-33_dp * EXP(725._dp/TEMP) * C_M
64 k46=k0+k3/(1+k3/k2)
65 END FUNCTION k46
66
```

S4 Supplementary Figures

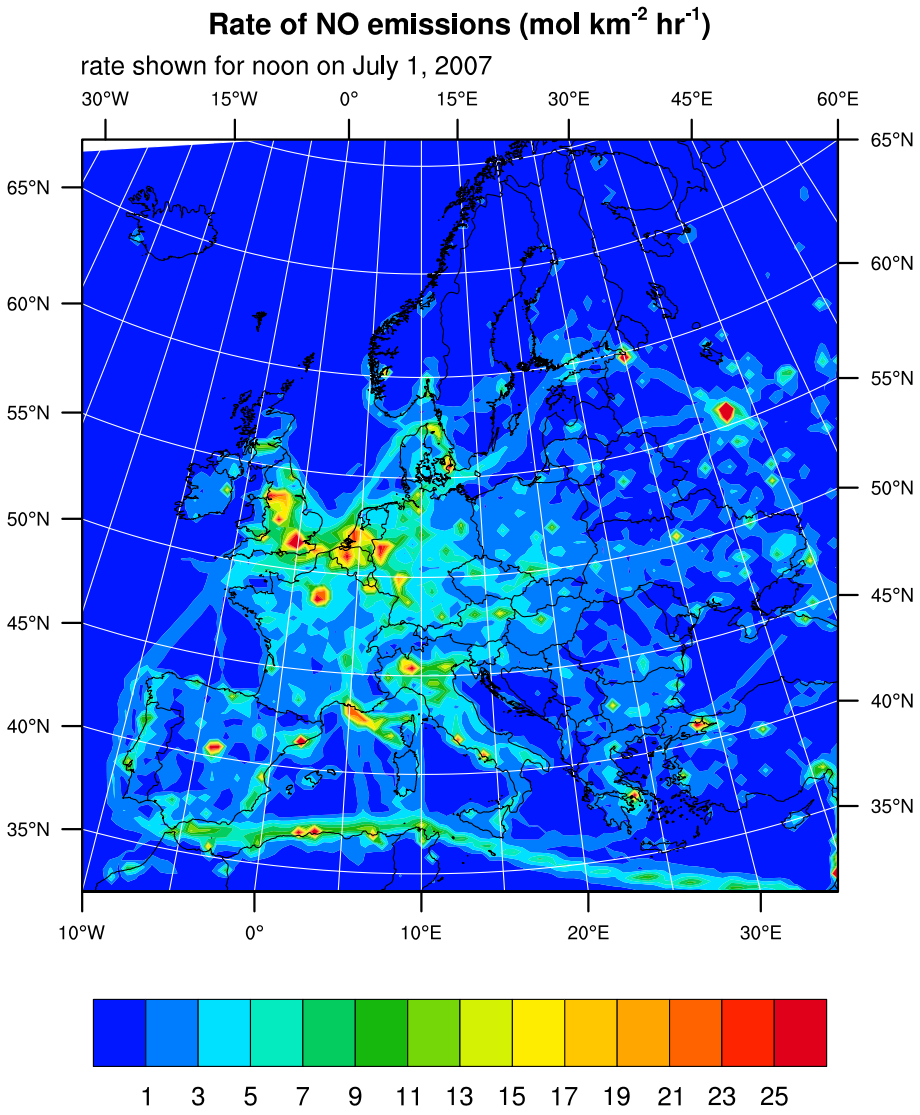

Figure S1: Example of NO emissions as processed for model input, combining the TNO-MACC II emissions inventory with the HTAP v2 inventory for the domain edges.

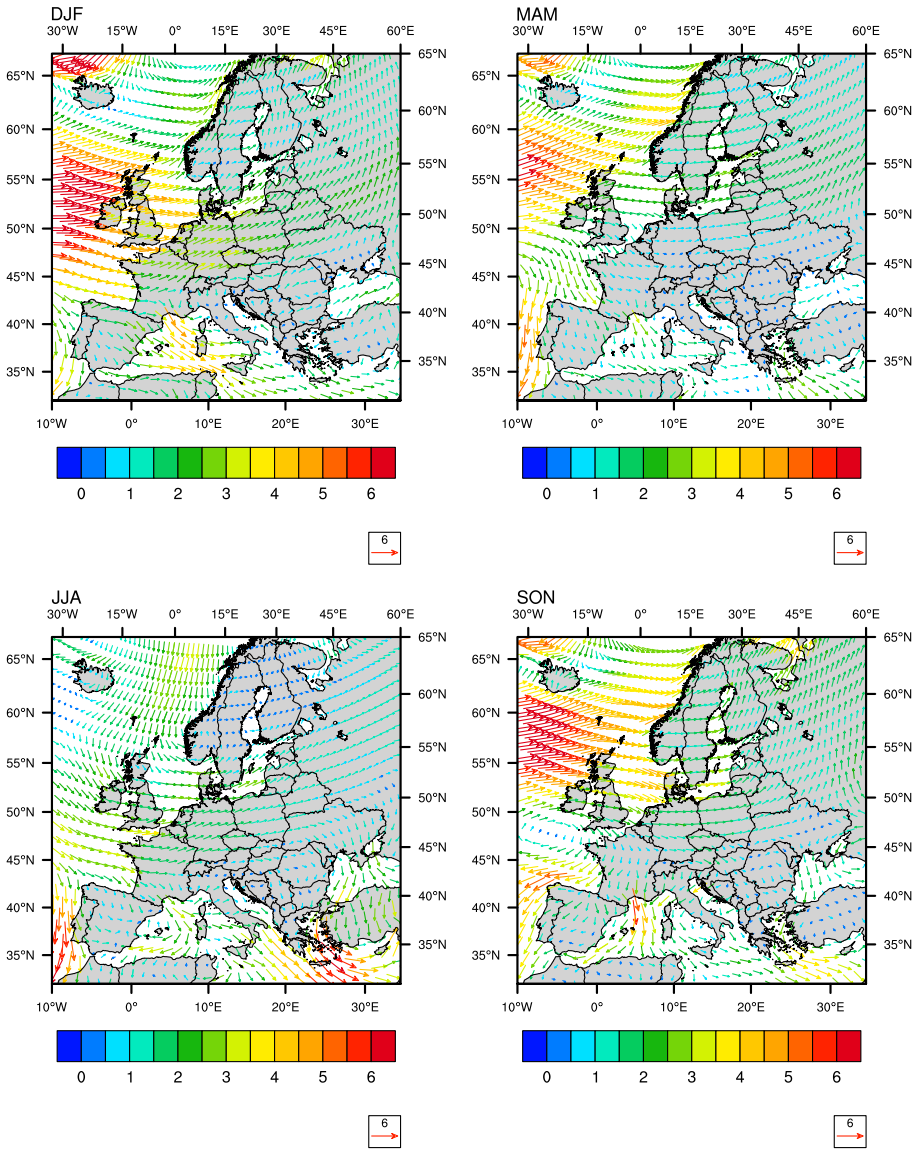

Figure S2: Seasonally-averaged wind vectors from ERA-Interim Reanalysis dataset for 2007, which used as meteorological forcing in our WRF-Chem simulations. Colors and vector length represent the wind speed in $\mathrm{m\,s^{-1}}$.

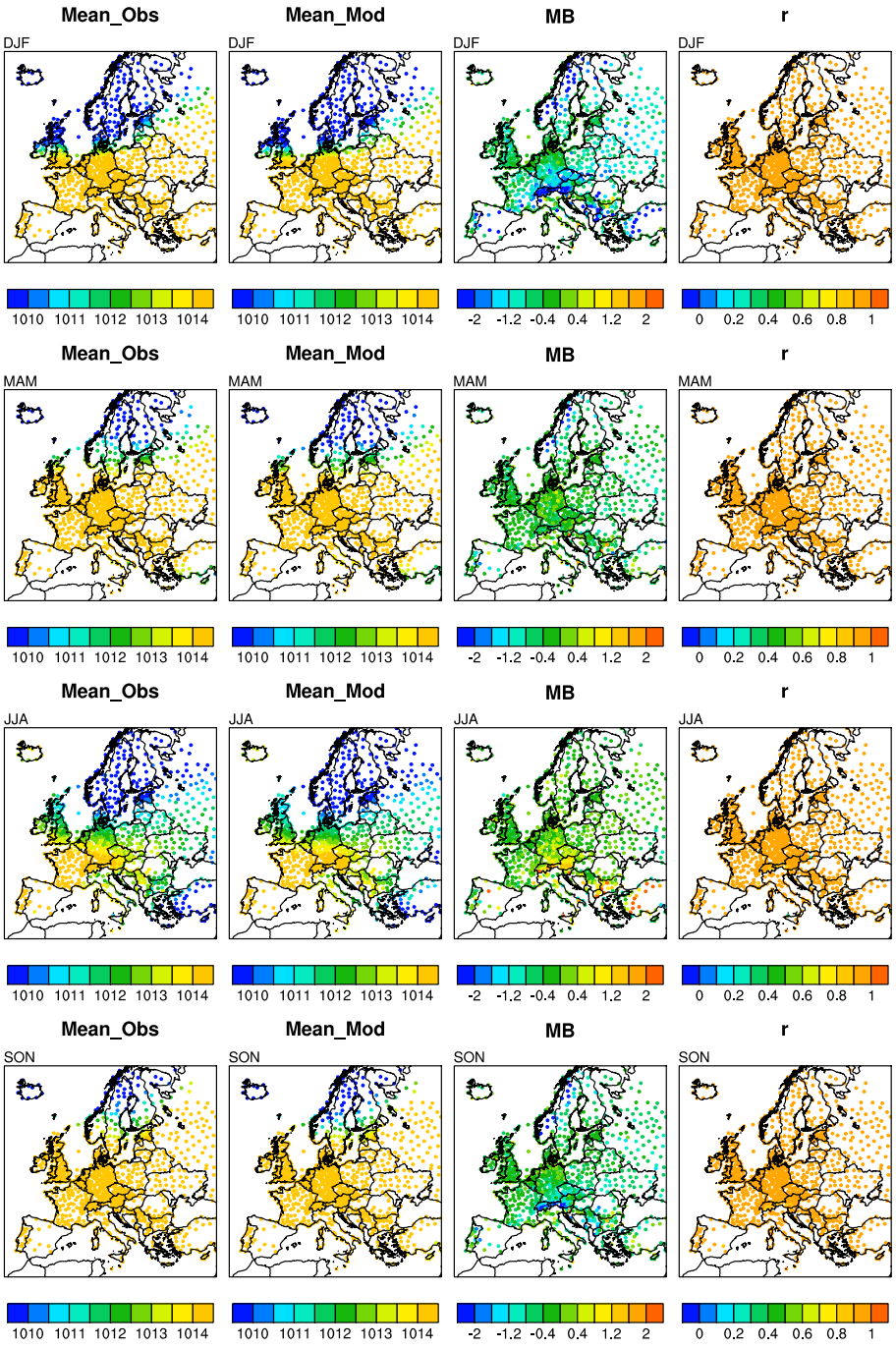

Figure S3: Seasonal average values of mean sea-level pressure (MSLP) in Pa. Model results from MOZART and statistics are shown at the locations of the observations.

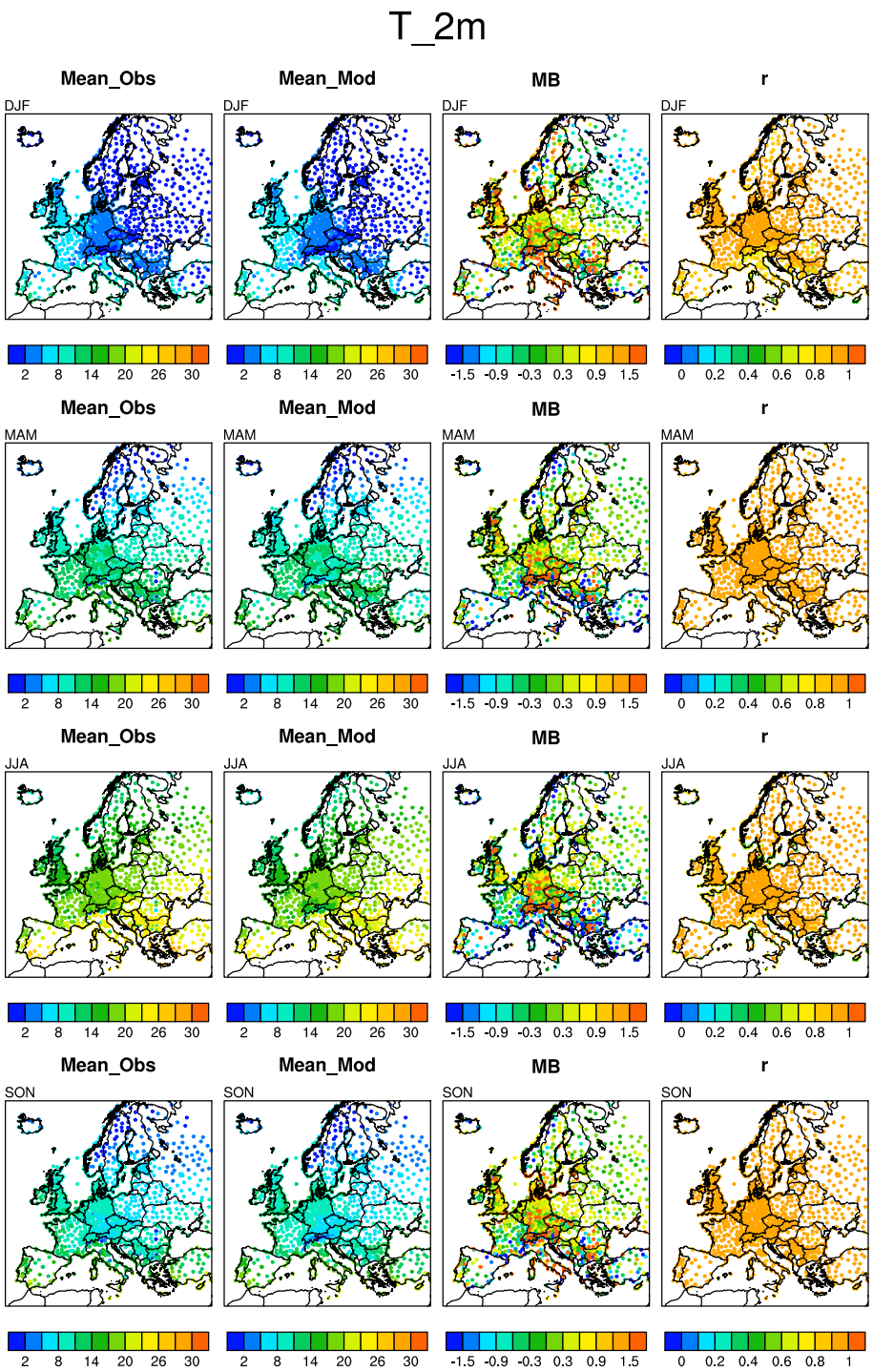

Figure S4: Seasonal average values of 2-meter temperature (T2) in degrees Celcius. Model results from RADM2 and statistics are shown at the locations of the observations.

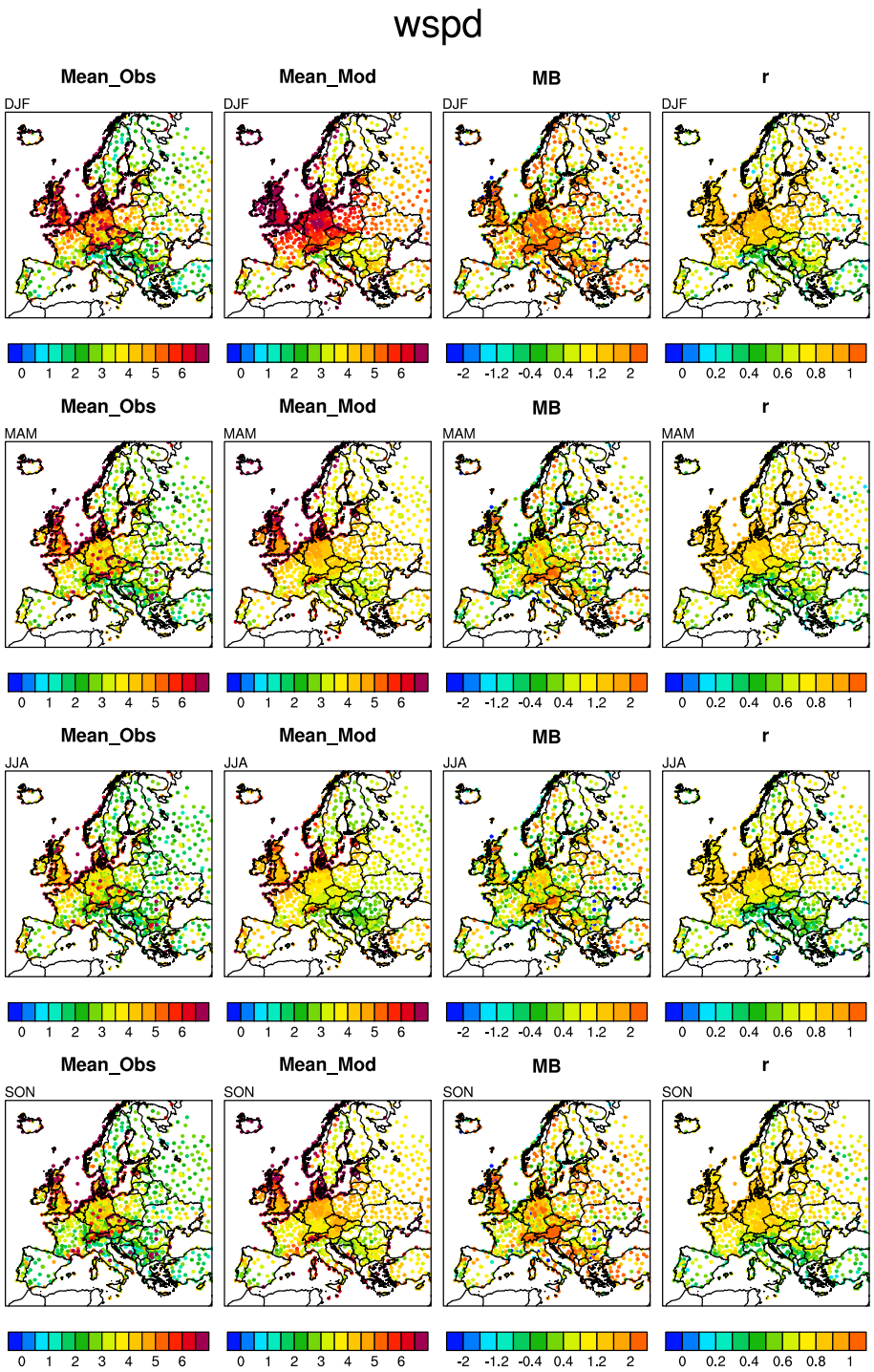

Figure S5: Seasonal average values of 10-meter wind speed (WS10) in m/s. Model results from RADM2 and statistics are shown at the locations of the observations.

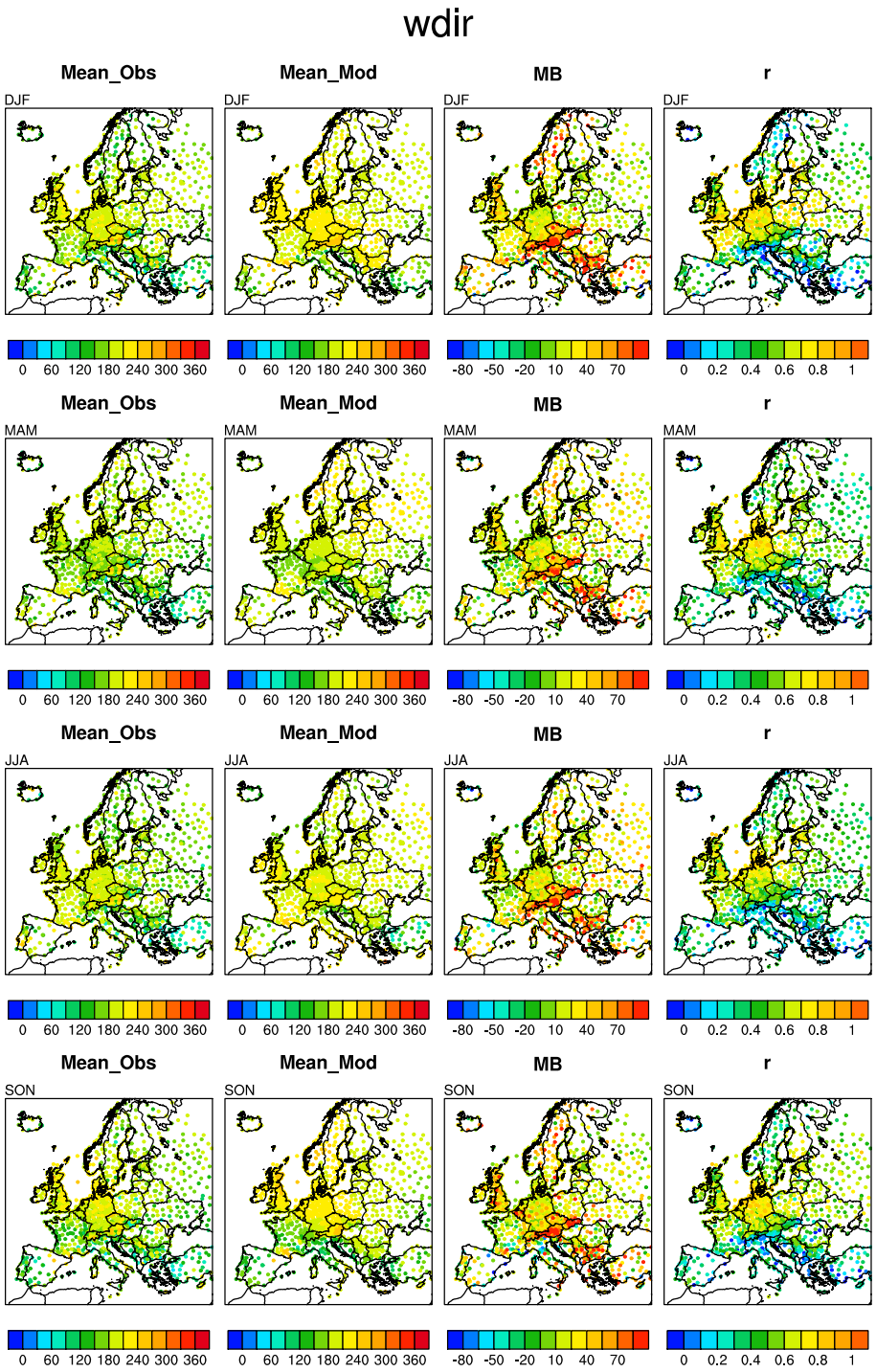

Figure S6: Seasonal average values of 10-meter wind speed (WS10) in m/s. Model results from RADM2 and statistics are shown at the locations of the observations.

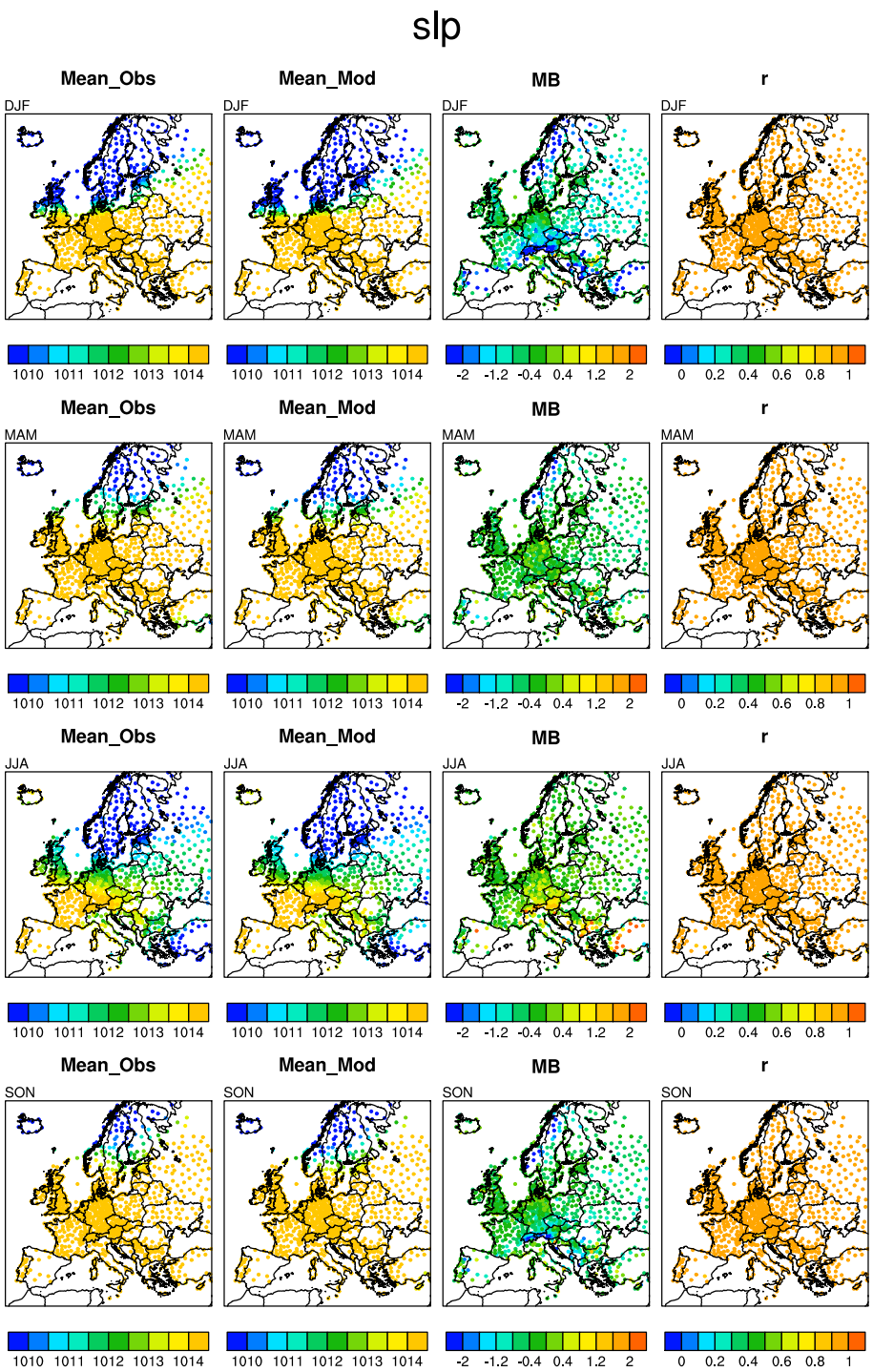

Figure S7: Seasonal average values of mean sea-level pressure (MSLP) in Pa. Model results from RADM2 and statistics are shown at the locations of the observations.

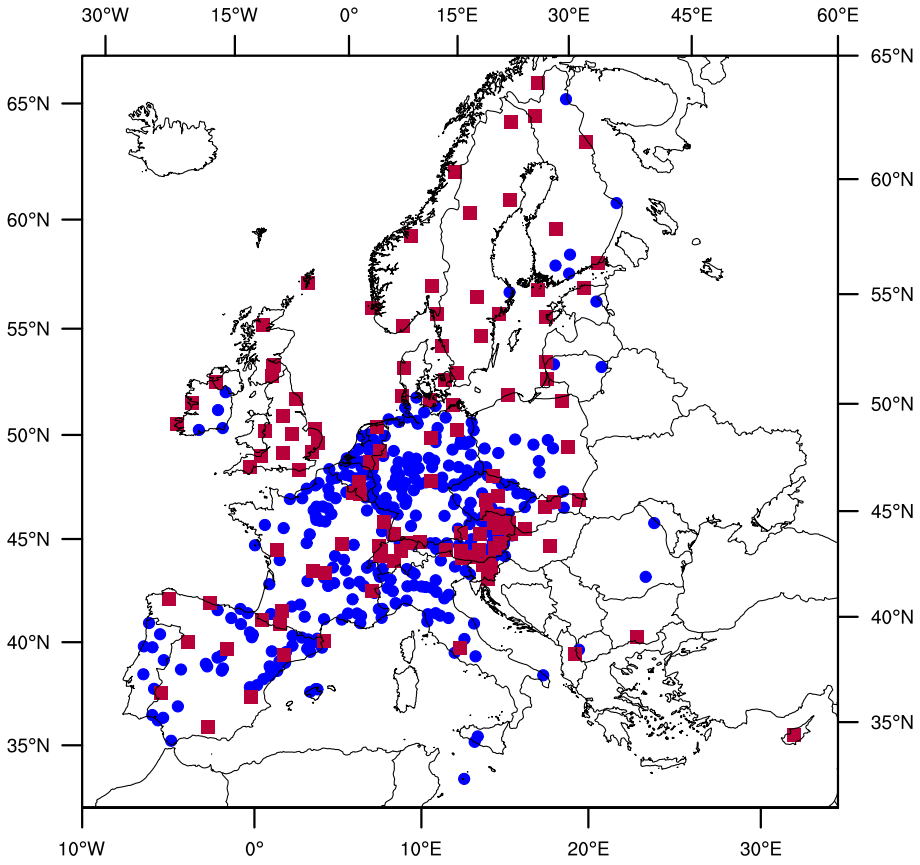

Figure S8: Location of AirBase (blue circles) and EMEP (red squares) observation sites. Shown here are stations which passed the completeness criteria for hourly O_3 measurements for summer 2007.

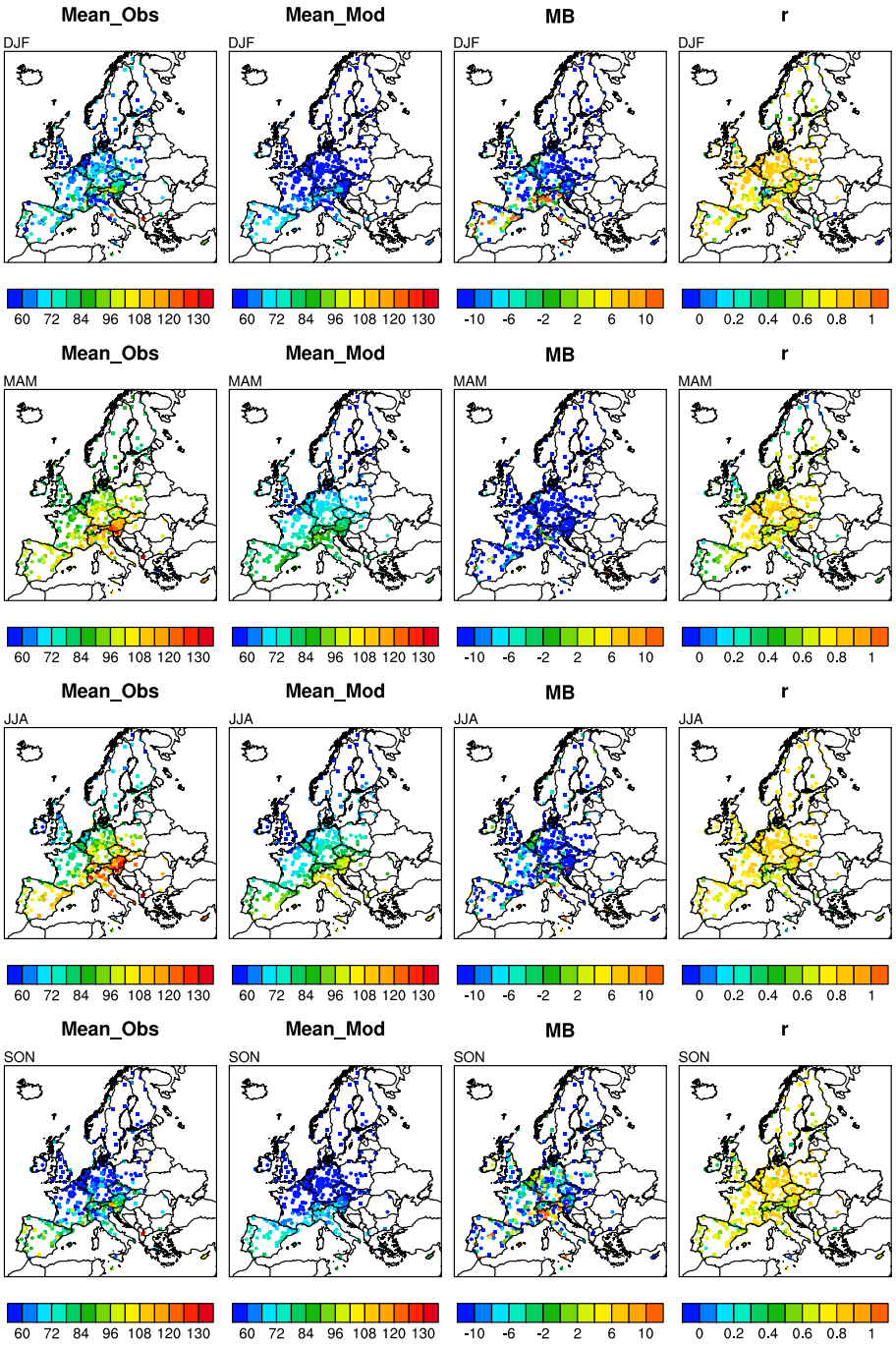

Figure S9: Seasonal average values of MDA8 in $\mu g\,m^{-3}$ calculated from hourly measurements at AirBase (circles) and EMEP (squares) stations, and modeled values from RADM2 for corresponding locations. The Mean Bias (MB, in $\mu g\,m^{-3}$) and temporal correlation coefficient (r) for daily values are also shown at the location of station observations.

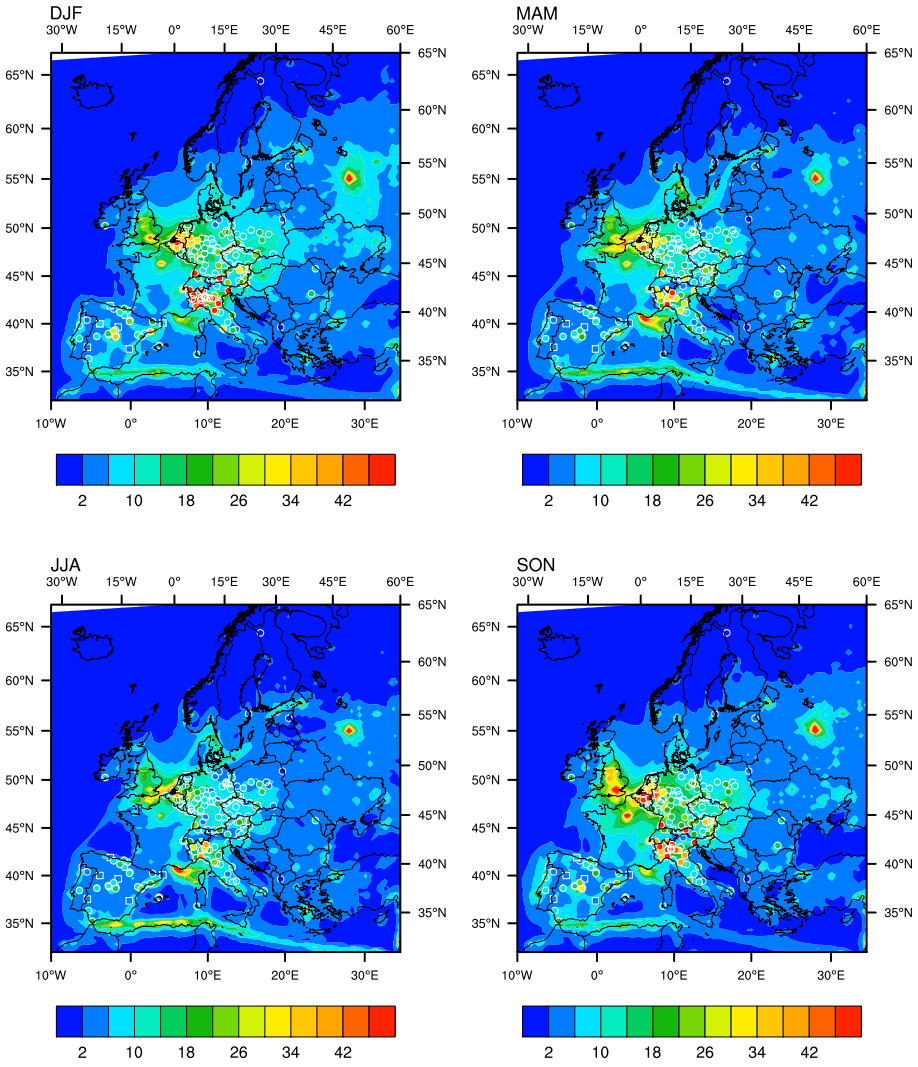

Figure S10: Seasonal average values of surface NO_x in $\mu g\,m^{-3}$. Contours are model output with the RADM2 mechanism. Filled dots represent hourly measurements at AirBase rural background stations, filled squares represent measurements at EMEP stations.

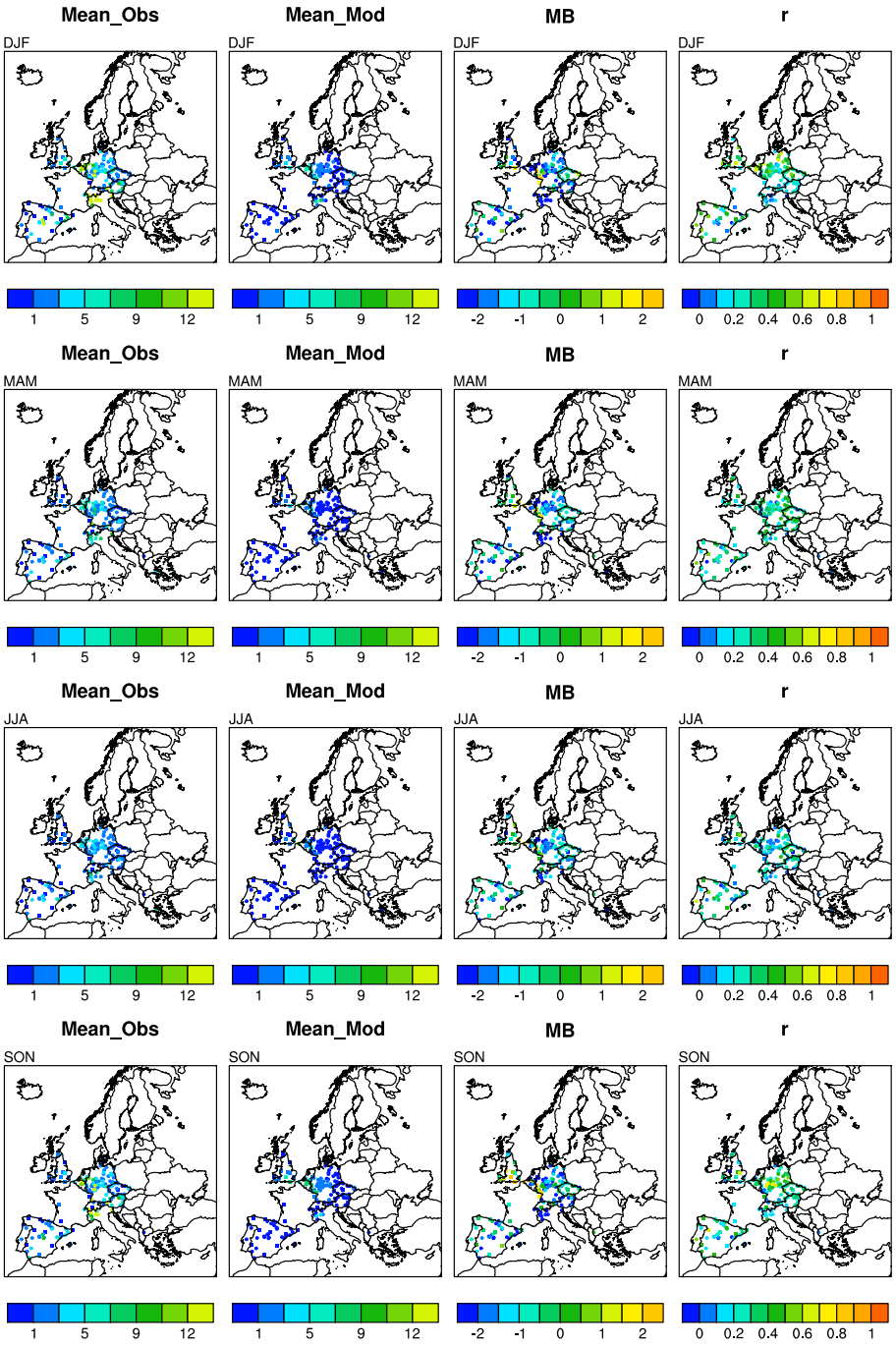

Figure S11: Seasonal average values of surface NO in µg m^{-3} from hourly measurements at AirBase (circles) and EMEP (squares) stations, and modeled values from RADM2 for corresponding locations. The Mean Bias (MB) and temporal correlation coefficient (r) for hourly values are also shown at the location of station observations.

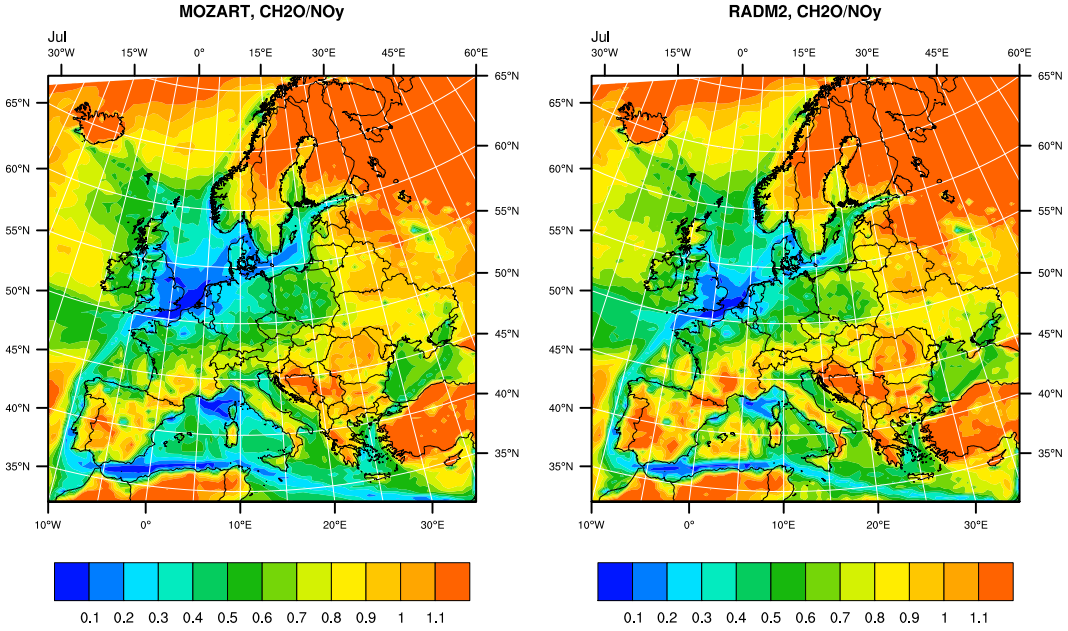

Figure S12: The spatial distribution of the monthly midday (11:00 - 14:00 CEST) ratio of CH_2O to NO_y. Following Sillman (1995), values of CH_2O/NO_y less than 0.28 indicated NO_x-saturated chemistry, and values greater than 0.28 indicate NO_x-sensitive chemistry.

References

J. W. Erisman, A. V. Pul, and P. Wyers. Parametrization of surface resistance for the quantification of atmospheric deposition of acidifying pollutants and ozone. *Atmospheric Environment*, 28(16):2595 – 2607, 1994. ISSN 1352-2310. doi: http://dx.doi.org/10.1016/1352-2310(94)90433-2. URL `http://www.sciencedirect.com/science/article/pii/1352231094904332`.

S. Sillman. The use of no y , h2o2, and hno3 as indicators for ozone-no x -hydrocarbon sensitivity in urban locations. *Journal of Geophysical Research: Atmospheres*, 100(D7):14175–14188, 1995. ISSN 2156-2202. doi: 10.1029/94JD02953. URL `http://dx.doi.org/10.1029/94JD02953`.

X. Tie, S. Madronich, S. Walters, R. Zhang, P. Rasch, and W. Collins. Effect of clouds on photolysis and oxidants in the troposphere. *Journal of Geophysical Research: Atmospheres*, 108 (D20):n/a–n/a, 2003. ISSN 2156-2202. doi: 10.1029/2003JD003659. URL `http://dx.doi.org/10.1029/2003JD003659`. 4642.

M. Wesely. Parameterization of surface resistance to gaseous dry deposition in regional-scale numerical models. *Atmospheric Environment*, 23:1293–1304, 1989. doi: doi:10.1016/0004-6981(89)90153-4.